Development of a Photoacoustic, Ultrasound and Fluorescence Imaging Catheter for the Study of Atherosclerotic Plaque

Maxime Abran, Guy Cloutier, *Senior Member, IEEE*, Marie-Hélène Roy Cardinal, Boris Chayer, Jean-Claude Tardif, and Frédéric Lesage

***Abstract*—Atherosclerotic cardiovascular diseases are a major cause of death in industrialized countries. Molecular imaging modalities are increasingly recognized to be a promising avenue towards improved diagnosis and for the evaluation of new drug therapies. In this work, we present an acquisition system and associated catheter enabling simultaneous photoacoustic, ultrasound and fluorescence imaging of arteries designed for *in vivo* imaging. The catheter performance is evaluated in tissue-mimicking phantoms. Simultaneous imaging with three modalities is demonstrated at frame rates of 30 images per second for ultrasound and fluorescence and 1 image per 13 seconds for photoacoustic. Acquired radio-frequency ultrasound data could be processed to obtain radial strain elastograms. With motorized pullback, 3D imaging of phantoms was performed using the three modalities.**

***Index Terms*—Biomedical electronics, biomedical optical imaging, catheters, fluorescence, molecular imaging, phantoms, photoacoustic effects, ultrasonic imaging.**

I. Introduction

CARDIOVASCULAR diseases (CV) are the main cause of mortality and morbidity worldwide [1]. The majority of CV events are related to atherosclerosis, a pathology characterized by the formation of a plaque into the artery wall [2]. Current challenges in evaluating the benefits of new drugs are associated with the difficulty of performing this evaluation on the background of effective standard therapy. To address this issue, new tools are needed to measure CV risk and to evaluate novel therapies. Potential candidates include imaging techniques, as they enable early and longitudinal measures of drug efficacy [3]. Current non-invasive imaging techniques include B-mode ultrasound, used to measure the carotid intima-media thickness (CIMT), computed tomography (CT), to quantify coronary and carotid calcium, and magnetic resonance imaging (MRI), to identify carotid fibrous cap status and to provide indirect measures of inflammation with magnetic contrast agents.

Intravascular ultrasound (IVUS) is a minimally invasive technique providing high-resolution images that allow the delineation of small plaques and the follow-up of remodeling processes, mainly in coronary arteries. Intravascular optical coherence tomography, which is a new technique, has recently been shown to provide better resolution than IVUS at the cost of a limited penetration (≈ 2 mm) [4]. It also necessitates a saline flush to reduce light absorption of blood.

Atherosclerosis imaging modalities presented above are mostly limited to depict structural features, but emerging molecular imaging techniques now offer an alternative to study the development of the plaque at a cellular level. Molecular imaging of atherosclerosis can provide relevant information on the development of the plaque with a large variety of biomarkers. For example, vascular cell adhesion molecule-1 (VCAM-1)-internalizing targeted iron oxide contrast agent showed greater uptake in the aorta of untreated hyperlipidemic apoE-knockout mice on a high-cholesterol diet compared to the statin-treated mice [5]. In our laboratory, anti-VCAM-1 was also successfully conjugated with a fluorophore or with gold nanoshells to provide photoacoustic contrast in mice [6]. Other targets (*e.g.*, matrix metalloproteinases [7], cathepsins [8], angiogenic markers [9]) have also been investigated. More recently, non-specific FDA approved indocyanine green (ICG), was shown to target lipid-loaded macrophages in human tissues *ex vivo* [10]. However, with optical imaging, most of the above studies were performed in mice due to the high absorption of light by the hemoglobin. For optical molecular imaging, extension to larger animals (rabbits, pigs) or humans requires an intravascular approach [10].

Multimodal imaging catheters combining ultrasound and photoacoustic were initially demonstrated with an external illumination thus preventing *in vivo* imaging [11], [12]. Fur-

Manuscript received March 21, 2014; revised July 08, 2014; accepted September 14, 2014. Date of publication October 24, 2014; date of current version November 06, 2014. This work was supported by a Canadian Institutes of Health Research (Lesage, Tardif, and Cloutier, 273578) and Natural Sciences and Engineering Research Council of Canada (NSERC, 239876-2011) discovery grant to F. Lesage, and a NSERC doctoral scholarship to M. Abran. This paper was recommended by Associate Editor S. Renaud.

M. Abran is with the Département de génie électrique and Institut de génie biomédical, École Polytechnique de Montréal, Montréal, QC H3C 3A7, Canada (e-mail: maxime.abran@polymtl.ca).

G. Cloutier is with the Laboratory of Biorheology and Medical Ultrasonics, Research Center (CRCHUM), University of Montréal Hospital, Montréal, QC H2X 0A9, Canada, and also with the Department of Radiology, Radio-Oncology and Nuclear Medicine, and Institute of Biomedical Engineering, University of Montréal, Montréal, QC H3C 3J7, Canada.

M.-H. R. Cardinal and B. Chayer are with the Laboratory of Biorheology and Medical Ultrasonics, Research Center (CRCHUM), University of Montréal Hospital, Montréal, QC H2X 0A9, Canada.

J.-C. Tardif is with the Montréal Heart Institute, Research Center, Montréal, QC H1T 1C8, Canada.

F. Lesage is with the Département de génie électrique and Institut de génie biomédical, École Polytechnique de Montréal, Montréal, QC H3C 3A7, Canada, and also with the Montréal Heart Institute, Research Center, Montréal, QC H1T 1C8, Canada (e-mail: frederic.lesage@polymtl.ca).

Color versions of one or more of the figures in this paper are available online at http://ieeexplore.ieee.org.

Digital Object Identifier 10.1109/TBCAS.2014.2360560

ther integration was demonstrated in recent works where an ultrasound catheter including an optical fiber was tested on phantoms [13]–[16] and used for *ex vivo* intravascular photoacoustic (IVPA)/IVUS imaging of a coronary artery [17]–[19]. Recently, an IVPA/IVUS imaging catheter was used for *in vivo* imaging of a rabbit, but with a low frame rate and on a ligatured artery [20]. Separately, 2D fluorescence imaging catheters were developed to perform molecular imaging of atherosclerotic plaques in rabbits [21]. Images were aligned with IVUS acquired with a different catheter, which complicated experimental acquisitions. Catheters combining IVUS and fluorescence imaging were also designed, but they remain relatively large in size [22]–[24].

In this work, we present the design and validation of a tri-modal catheter, combining photoacoustic, ultrasound and fluorescence imaging. Data from all three modalities are acquired and displayed simultaneously and the scanning system is designed for *in vivo* imaging. Furthermore, achieved image acquisition at a frame rate of up to 30 Hz in IVUS enables intravascular elastography (IVE) applications. The IVE method displays tissue deformations produced by the pulsating blood pressure using radio-frequency IVUS images. It has been shown to have potential to identify plaque components and vulnerability [25], [26]. In this work, the diameter of the optical fiber and transducer assembly is 1.1 mm. When inserted in a catheter sheath, it has an outer diameter of 1.4 mm, small enough to fit in a 5 French introducer. The design of the system and its validation in tissue-mimicking phantoms are described including tri-modal 2D and 3D images.

II. Materials and Methods

A. System Overview

The system was designed as an ultrasound-optical imaging catheter linked to an optical assembly and custom-made electronics. The catheter per se combined an optical fiber for fluorescence imaging and photoacoustic excitation and an ultrasound transducer for acoustic imaging and detection of photoacoustic signals. The electronic circuit synchronized the acquisition of the three modalities with the two motors driving the rotating/translating catheter assembly. The raw data was then transferred to a laptop via a USB connection at rates up to 250 Mbps. A Matlab user interface filtered the signals, reconstructed and displayed the three images in real time during acquisitions.

B. Catheter Conception

Catheters were built by gluing an optical fiber to an ultrasound transducer and its transmission cable with cyanoacrylate along the full length of the catheter. The ultrasound transducer single element and its coaxial transmission cable were extracted from a commercial IVUS 45 MHz catheter (Revolution, Volcano Therapeutics, Rancho Cordova, CA, USA). The $400\ \mu\mathrm{m}$ optical fiber had a numerical aperture of 0.22. A $500\ \mu\mathrm{m}$ right angle prism with an aluminized hypotenuse (Edmund Optics Inc., Barrington, NJ, USA) was glued at the tip of the fiber for side-fire illumination with an optical UV curing adhesive.

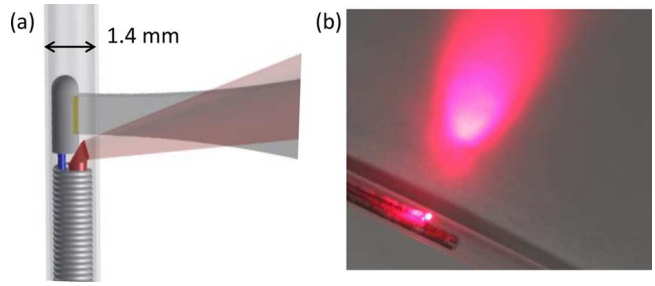

Fig. 1. (a) Diagram of the tip of the catheter. The overlapping region of the light illumination and the ultrasound field of view is shown. It allows the co-registration of the different imaging modalities. The space under the prism and between the fiber and the transducer is filled with glue. (b) Photograph of the tip of the catheter inside the LDPE tube. The fiber was connected to a 660 nm laser and the catheter was placed on a white surface for visualization.

Alignment was performed by gluing the optical fiber and the ultrasound transducer under a microscope. The prism was tilted on the tip of the fiber by about 15 degrees, to optimize the overlapping region of the illumination and ultrasound emission. This region starts at 1.5 mm from the catheter's surface. The assembly was inserted inside a customized torque coil (Asahi Intecc, Santa Ana, CA, USA) to obtain a uniform rotation and then installed in a thin low-density polyethylene (LDPE) tube with an outer diameter of 1.4 mm so that it would fit in a 5 French introducer. The rigidity of the optical fiber added negligible distortion in the IVUS signal due to the non-uniform rotation, even when applying a radius of curvature of 30 mm. The catheter had a length of 150 cm. A diagram and a picture of the tip of the catheter are shown in Fig. 1.

A DC motor (MicroMo, Clearwater, FL, USA) was used to rotate the optical fiber and the ultrasound transducer at an angular speed of 30 revolutions/second. Two hundred fifty six angular positions were acquired at each revolution to generate the images. A linear motor (Zaber Technologies, Vancouver, BC, Canada) was used to add a pullback function and to enable 3D reconstructions. Optical and electrical connections between the fixed and rotating assemblies used an optical rotary joint for the optical fiber (Doric Lenses, Quebec, QC, Canada) and a slip ring to transmit and receive the electrical signals, both able to operate at 30 revolutions/second. A small preamplifier with a gain of 20 dB was designed to rotate with the ultrasound transducer to amplify the signal close to the source. A transmit/receive switch was installed in front of the preamplifier to protect the amplifier circuit from the pulser. The slip ring had extra signal lines to provide power to this circuit. The ultrasound excitation signal and the output of the preamplifier were transmitted to the main acquisition circuit through the slip ring.

C. Optical Design

Fig. 2 provides an overview of the optical system, combining photoacoustic illumination and fluorescence imaging.

For photoacoustic imaging, a Q-switched ND:YAG pulsed laser (Quanta-Ray INDI series, Newport Corporation, Irvine, CA, USA), followed by an Optical Parametric Oscillator (OPO, GWU-Lasertechnik, Erftstadt, Germany), operating at 710 nm was used. The repetition rate of the laser was 20 Hz and it was synchronized with the rotating motor. The pulse energy was

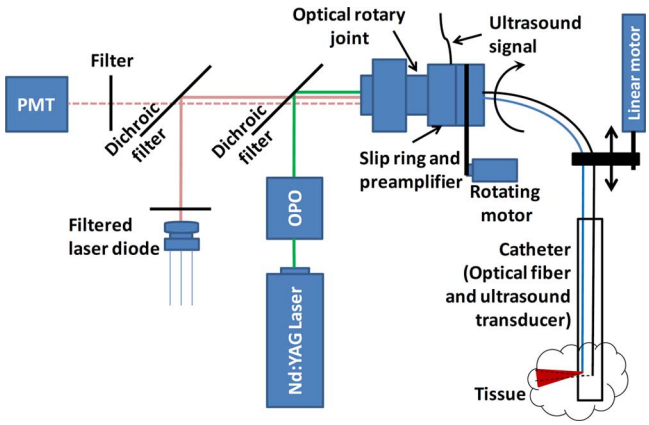

Fig. 2. Overview of the tri-modal catheter system.

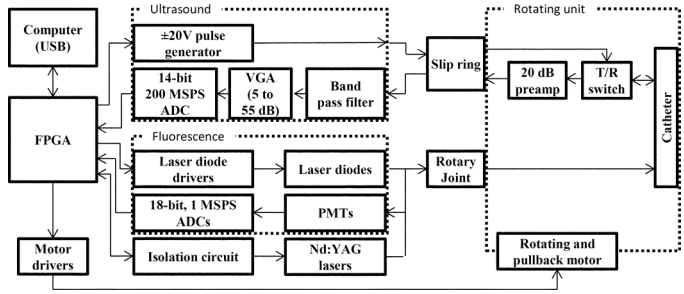

Fig. 3. Block diagram of the electronic circuit.

$150\ \mu$J at the tip of the catheter. The laser did not cause any damage to the prism or the fiber. We have calculated that the fluence on an artery wall at 1 mm from the catheter through blood would be $3\ \mathrm{mJ/cm^2}$, which is below the ANSI safety limit of $20\ \mathrm{mJ/cm^2}$.

For fluorescence imaging, a filtered laser diode ($\lambda = 780$ nm, filter: 769 ± 20 nm) was used to excite the fluorophore. The output power at the tip of the catheter was 25 mW. A photomultiplier tube (PMT, Hamamatsu Photonics, Hamamatsu City, Japan), combined with a narrow-band optical filter (832 ± 19 nm) was used to detect the emitted fluorescence. A dichroic filter (cut-off wavelength: 801 nm) isolated the excitation and emission light paths. Filter sets can be changed depending on the fluorophore, in the experiments below, ICG was used. A second dichroic filter (cut-off wavelength: 741 nm) was placed between the fluorescence and photoacoustic light paths to maximize light transmission for both modalities and to avoid saturating the PMT during photoacoustic pulses.

D. Electronics

The electronic circuit was custom designed from discrete electronic parts to allow simultaneous tri-modal imaging. The main component of the system was a field-programmable gate array (FPGA) (Cyclone III, Altera, San Jose, CA, USA) linked to the computer by a USB connection (using a microcontroller from Cypress Semiconductor, San Jose, CA, USA). The FPGA was in charge of synchronizing and recording all signals acquired. Analog electronics for ultrasound pulse-echo, fluorescence detection and motor control were also integrated and controlled by the FPGA. The schematics of the entire electronic circuit are available on demand.

The ultrasound excitation was generated by a ± 20 V custom pulse circuit with a return-to-zero function. Photoacoustic and ultrasound detection circuits included a variable-gain amplifier (VGA) with customizable time-gain compensation and a 14-bit analog-to-digital converter (ADC) acquiring at 200 MegaSamples/second. The circuit further included digital lines for control of the Nd:YAG laser.

For fluorescence imaging, a laser driver circuit allowed flexibility in using almost any laser diode, depending on the fluorophore used. The variable gain PMT was amplified and then digitalized at 250 kiloSamples/second using an 18-bit ADC. Finally, a part of the circuit controlled the speed of the DC rotating motor and the position of the linear pullback motor. The system included two laser driver and PMT acquisition circuits to visualize two fluorescent contrasts simultaneously for future works.

All data acquired was relayed in real-time to the computer at every angular position. A packet of data contained an ultrasound and photoacoustic vector, a fluorescence value and other acquisition information, such as the motor positions, errors and warnings.

E. Acquisition

Data in ultrasound and fluorescence modes were acquired at a frame rate of 30 Hz. Due to the limited pulse rate of the photoacoustic laser ($20\ \mathrm{Hz} \pm 1\ \mathrm{Hz}$), obtaining a full frame in this modality required 13 seconds. At this laser repetition rate, a photoacoustic laser pulse and acquisition could be performed every 1 turn and a half (i.e., for 256 angles, $\theta_1 = 1$, then $\theta_2 = 129$, $\theta_3 = 2$, $\theta_4 = 130$, $\theta_5 = 3$, etc.). Laser triggering by the acquisition system in the range 19-21 Hz allowed synchronisation between angular positions (measured by the encoder of the motor) and precise angular pulse triggering. In future developments, it would be feasible to increase the frame rate by using lasers pulsing at kHz rates without any changes to the system electronics or software.

The acquisition process for each angular position is presented in the timeline of Fig. 4. First, a trigger was sent to the Nd:YAG laser to illuminate the tissue and the photoacoustic signal was recorded. Next, an ultrasound pulse was generated with the transducer, and the associated echo was recorded to form an ultrasound RF line. Five ultrasound echoes could be performed before the motor reached a new position (adjustable depending on the rotation speed). This specification is of interest if one aims to improve the signal-to-noise ratio (SNR) of B-mode images by reducing the rotation speed. The fluorescence excitation and recording started just after the Nd:YAG laser pulse and lasted until a new angular position.

F. Reconstruction

At each angular position, the FPGA sent the acquired data to a Matlab user interface on the acquisition computer. When a complete slice of 256 angular positions was received, a B-mode image was reconstructed for visualization. For that purpose, photoacoustic and ultrasound data were processed first with a band-pass filter (4th order Butterworth, 40 to 50 MHz), followed by a Hilbert transform. Ultrasound data was processed with a

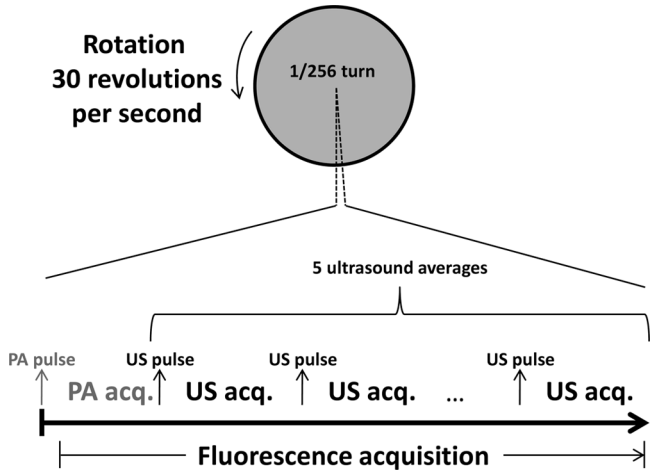

Fig. 4. Timeline of the tri-modal acquisition for a single angular position repeated 256 times to gather one frame. A frame rate of 30 Hz could be obtained with the current implementation. The photoacoustic (PA) pulse and acquisition was not generated at every angular position, but at 20 Hz on average.

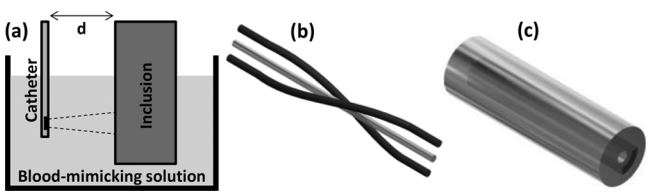

Fig. 5. 3D depiction of the phantoms. (a) Phantom for fluorescence and photoacoustic sensitivity tests ('d' is an adjustable distance from the outer layer of the catheter to the thin film of the surface of the inclusion). The inclusion contained either ICG or black ink at different concentrations. (b) Two tubes in a spiral shape (one filled with ICG and the other with black ink) around the imaging catheter for tri-modal validation. (c) PVA phantom with a softer region on one quarter of a slice for ultrasound elastography measures. This region was injected with ICG for fluorescence validation.

logarithm compression. The dynamic range of the signal was 59 dB before logarithm compression and 20 dB after. Further, the images were converted from polar coordinates to Cartesian coordinates. Slices from the three modalities were displayed in real time during the acquisition at up to 30 images/second. For 3D reconstructions, an isosurface with a threshold value was applied to generate the images presented below.

G. Phantoms

To measure the sensitivity of the system, we placed an inclusion at various distances from the catheter in a blood-mimicking solution, as seen in Fig. 5(a). The inclusion was a rectangular-shaped container with a thin and transparent plastic wall. The container had a depth and a width of 10 mm. It contained either ICG at 100 nM and 1 μM or black ink dilutions to measure fluorescence and photoacoustic sensitivity, respectively.

To validate the tri-modal imaging capabilities, we placed two tubes shaped in a spiral around the catheter in the blood-mimicking solution, as seen in Fig. 5(b). The diameter of the spiral was about 5 mm. Tubes were made of low density polyethylene (LDPE) with an internal diameter of 1.2 mm. To generate photoacoustic and fluorescence contrasts, one of the tubes was filled with ICG at 1 μM and the other with black ink.

To evaluate the capability of performing ultrasound elastography imaging, a tissue-mimicking phantom was made using a mix of 10% polyvinyl alcohol (PVA, #CAS7732–18-5, Beacon, NY, USA) dissolved in pure water and ethanol homopolymer (#CAS9002–89-5), and 2% of Sigmacell cellulose particles (type 20, Sigma Chemical, St-Louis, MO, USA). Sigmacell acted as both acoustic and optical scatterers. Black ink was added to the PVA solution for optical absorption. The phantom is shown in Fig. 5(c). It was shaped as a hollow cylinder with an outer diameter of 15 mm, an inner diameter of 4 mm and a length of 30 mm. A 3D printer (Replicator 2X, Makerbot, Brooklyn, NY, USA) was used to make the moulds and allowed the construction of reproducible phantoms. The phantom underwent 6 freeze-thaw cycles to induce the desired solidification and polymerization of the PVA [27]. It contained a sub-section that underwent a single freeze-thaw cycle, which led to a softer region. This region represented 90 degrees of a slice, positioned from 3 mm to 5 mm radial distance from the center. During experiments, this phantom was filled with a blood-mimicking solution and connected to a dynamic pump simulating the pulsatile blood pressure of the heart at 100 beats per minute (model #1421, Harvard, Holliston, MA, USA). Since the number of freeze-thaw cycles has little effect on the echogenicity of the phantom, the sub-section was not expected to be visible in B-mode. However, elastography aimed to detect changes in stiffness of the phantom by analysing consecutive RF images during pulsation with the Lagrangian speckle model estimator [28]. The sub-section was also injected with 1 μM of ICG, to allow fluorescence co-localization.

In all phantom experiments, the blood-mimicking solution was 1% intralipid and 0.1% black ink diluted in water to obtain a reduced scattering coefficient of $\mu_s' = 1\ \mathrm{mm}^{-1}$ and an absorption coefficient of $\mu_a = 0.5\ \mathrm{mm}^{-1}$ [29]. No ultrasound scatterers were present in the lumen of the phantom (*i.e.*, in the circulating blood-mimicking fluid of Fig. 5(c).

III. Results

A. Sensitivity Measurements

Sensitivity measurements in photoacoustic and fluorescence imaging were performed with an inclusion at various distances from the catheter in a blood-mimicking solution. Signal-to-noise ratios (SNR) were calculated and the results are shown in Fig. 6. The catheter was rotating at 30 revolutions/second and both SNRs were calculated using the signal of a single frame (no averaging). Higher SNR could be achieved by averaging multiple frames (results not shown). SNR was calculated by dividing the signal amplitude by the standard deviation of the background in a region where there were no inclusions.

In fluorescence, 100 nM & 1 μM of ICG were detected through a blood-mimicking solution at up to 1.4 mm and 2.8 mm, respectively. Black ink was visible in photoacoustic through 5 mm of blood-mimicking solution. IVUS images were used to measure the distance between the outer layer of the catheter and the beginning of the inclusion.

In the sensitivity measurements shown above, we used a blood-mimicking solution with $\mu_s' = 1\ \mathrm{mm}^{-1}$ to gather results

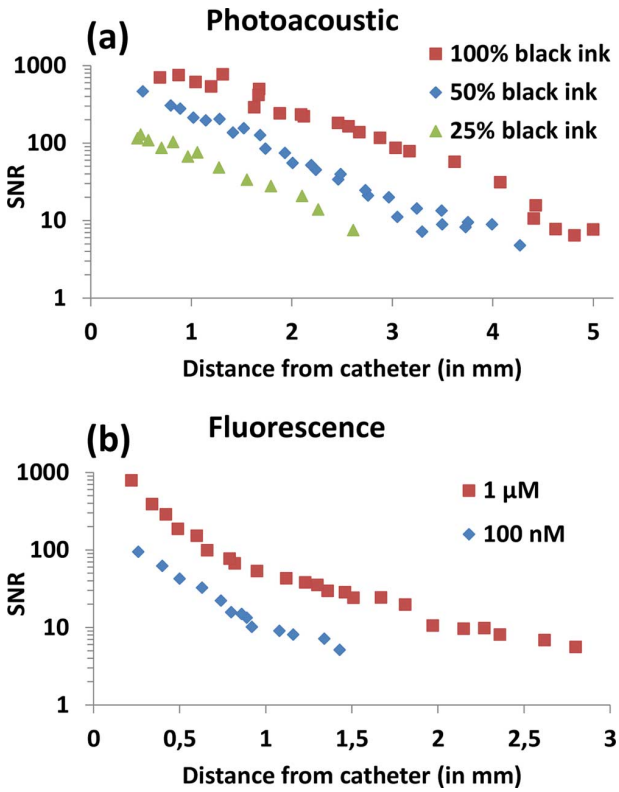

Fig. 6. (a) Sensitivity in photoacoustic with black ink at different concentrations. The ink was diluted in water for the 50 and 25% concentrations. (b) Sensitivity in fluorescence with different concentrations of indocyanine green. Dilutions were made with dimethyl sulfoxyde.

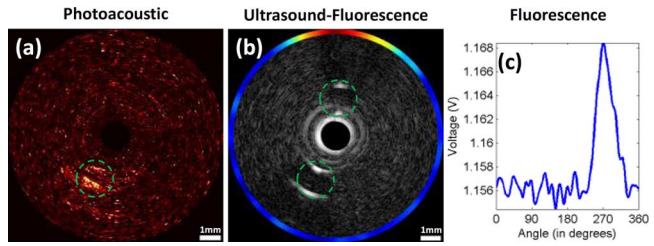

Fig. 7. Simultaneous photoacoustic, ultrasound and superimposed fluorescence imaging. (a) The bottom inclusion (tube filled with black ink) is visible in photoacoustic. (b) Both inclusions are visible in IVUS. The contour in the IVUS image represents the fluorescence intensity signal. The top inclusion (tube filled with 1 μM of ICG) is visible in fluorescence. (c) Fluorescence signal is shown. 0° is at the right of the IVUS image, with a clockwise rotation.

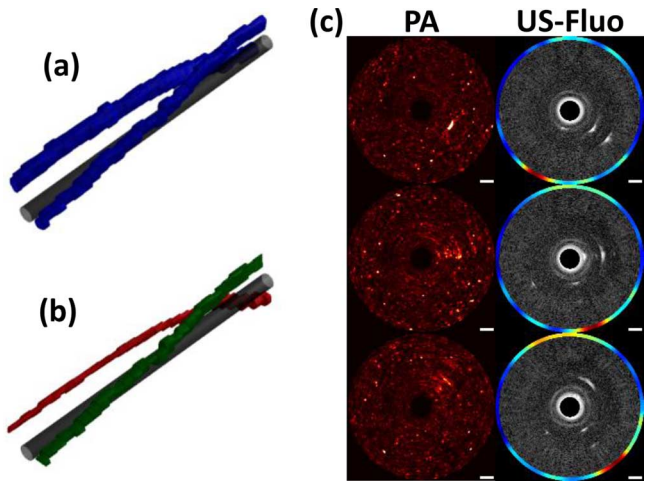

Fig. 8. 3D reconstructions from a tri-modal acquisition. The catheter is shown in gray. (a) Ultrasound signal of both inclusions is in blue. (b) Photoacoustic signal is in red and fluorescence signal in green. (c) 3 frames along the phantom in all three imaging modalities. Scale bar is 1 mm.

comparable with previous work [30], but this value slightly underestimated blood scattering. We performed Monte Carlo photon propagation simulations with a more realistic value of $\mu_s' = 3\ \mathrm{mm}^{-1}$ to assess the impact on our sensitivity measures. Using higher scattering, the fluorescence signal intensity is expected to be reduced by 65% according to simulations. Therefore, an average of 8 frames would be required to obtain the SNR shown. However, in an *in vivo* experiment, this would not be detrimental, as it corresponds to a longitudinal length of 0.13 mm, well below the resolution achievable by this modality, at a pullback speed of 0.5 mm/s and given our rotation speed of 30 revolutions/second.

B. Tri-Modal 3D Imaging Validation

In Fig. 7, simultaneous photoacoustic, fluorescence and ultrasound imaging on a slice of the phantom in Fig. 5(b) is shown.

It took 13 seconds to acquire the photoacoustic signal without averaging (single shot for each angle), while the ultrasound and fluorescence signals were from a single frame acquired at 30 frames/second. The system differentiated photoacoustic and fluorescent contrasts without any apparent crosstalk. In IVPA, the signal is not as strong closer to the catheter, due to the overlapping region of the illumination and ultrasound beam, which starts at 1.5 mm from the catheter. We measured an axial resolution of 80 μm in IVUS. The phantom used for tri-modal imaging validation was not the same as the one used for sensitivity measurements. Therefore, obtained SNRs differ between both results as they are dependent on the spatial sensitivity associated with light propagation.

To demonstrate the feasibility of three-dimensional imaging, the same phantom was imaged, while performing a 30 mm pullback. Fig. 8 shows a 3D reconstruction obtained from photoacoustic, fluorescence and ultrasound images.

The 3D images were built using 30 slices taken at every 1 mm. The total acquisition time was 7 minutes (effective pullback speed of 0.07 mm/s). 3D fluorescence was achieved by using the ultrasound image as a prior to obtain the depth of the inclusion [31].

C. Elastography

The inner and outer contours of the phantom images were segmented using a fast marching algorithm based on a combination of gray level gradient and mixtures of gamma probability density functions (PDFs) to model the log-compressed envelop gray level distribution of the IVUS [32].

IVE elastograms were computed for the segmented phantom wall according to the polar domain Lagrangian speckle model estimator that provides the radial and circumferential strains and

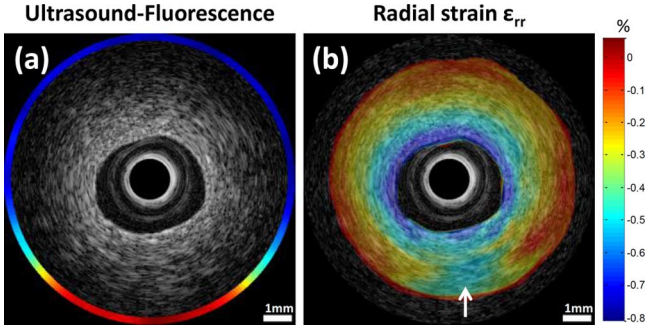

Fig. 9. (a) Combined IVUS-fluorescence image of a slice of the phantom. (b) Radial strain deformation in %. The softer region is shown by the white arrow. Negative strains correspond to the compression of the phantom.

shears [26]. The latter implementation compensated possible artifacts attributed to the eccentricity of the catheter within the vessel lumen. Vessel wall deformations were estimated in percent between two consecutive temporal RF IVUS images. For each elastogram, tissue displacements and their spatial derivatives were computed with an optical flow algorithm between corresponding cross-correlated small regions of interest (ROIs) from both images. The radial and circumferential strains and shears were then determined from those values; see [26] for additional details.

In this study, the radial strain ε_{rr} was used to characterize the phantom elastic properties, as depicted in Fig. 9(b). ROIs of 0.58 mm radially and 0.74 radian circumferentially were used. As expected, larger radial strains were computed close to the lumen contour; these strains decreased in magnitude as a function of depth (strain decay phenomenon) except for the softer inclusion shown at 6 o'clock where higher radial strains were measured.

As expected, the soft inclusion was not visible in a static B-mode IVUS image because the number of freeze-thaw cycles had little effect on the density and compressibility of the PVA (*i.e.*, on the acoustic impedance). However, the elastography analysis could detect the inclusion zone and co-localization was seen with fluorescence imaging.

IV. Conclusion

In this work, we demonstrated a tri-modal acquisition system and catheter providing simultaneous images in all tested modalities, RF IVUS data of good quality for elastography measures, and a design ready for *in vivo* acquisitions. Two imaging modalities can be used for molecular imaging (fluorescence and photoacoustic) and, when combined to an IVUS catheter, this technique may be amenable to image multiple molecular targets *in vivo*.

In fluorescence and photoacoustic, the sensitivity measurements and the penetration depth suggested that *in vivo* intravascular imaging may be possible. With photoacoustic imaging, the frame rate remained realistic for *in vivo* pre-clinical use (13 seconds/frame) but this could be improved by the use of more powerful and faster excitation sources, available on the market, to help increase IVPA SNR and frame rate.

Previous multimodal catheters reported frame rates of less than 10 images/second in fluorescence imaging with a larger catheter than us [22]–[24]. Our scanning system and catheter allowed colocalized acquisitions of fluorescence and ultrasound at a frame rate of 30 images/second. We further integrated the optical fiber inside the catheter, reducing the diameter to 1.4 mm, which is small enough to fit inside a 5 French introducer and image the aorta of a rabbit. To our knowledge, we presented the first intravascular catheter combining fluorescence and elastography imaging, the latter requiring a high frame rate.

The sensitivity of the system with molecular probes *in vivo* remains to be evaluated. Our next steps will be to extend this work to *in vivo* studies and confirm the potential of this technology for atherosclerotic plaque characterization.

References

[1] A. D. Lopez, C. D. Mathers, M. Ezzati, D. T. Jamison, and C. J. Murray, "Global and regional burden of disease and risk factors, 2001: systematic analysis of population health data," *The Lancet*, vol. 367, no. 9524, pp. 1747–1757, May .

[2] M. Naghavi, P. Libby, E. Falk, S. W. Casscells, S. Litovsky, J. Rumberger, J. J. Badimon, C. Stefanadis, P. Moreno, G. Pasterkamp, Z. Fayad, P. H. Stone, S. Waxman, P. Raggi, M. Madjid, A. Zarrabi, A. Burke, C. Yuan, P. J. Fitzgerald, D. S. Siscovick, C. L. De Korte, M. Aikawa, K. E. J. Airaksinen, G. Assmann, C. R. Becker, J. H. Chesebro, A. Farb, Z. S. Galis, C. Jackson, I.-K. Jang, W. Koenig, R. A. Lodder, K. March, J. Demirovic, M. Navab, S. G. Priori, M. D. Rekhter, R. Bahr, S. M. Grundy, R. Mehran, A. Colombo, E. Boerwinkle, C. Ballantyne, W. Insull Jr., R. S. Schwartz, R. Vogel, P. W. Serruys, G. K. Hansson, D. P. Faxon, S. Kaul, H. Drexler, P. Greenland, J. E. Muller, R. Virmani, P. M. Ridker, D. P. Zipes, P. K. Shah, and J. T. Willerson, "From vulnerable plaque to vulnerable patient: a call for new definitions and risk assessment strategies: Part I," *Circulation*, vol. 108, no. 14, pp. 1664–1672, Oct. 2003.

[3] J.-C. Tardif, F. Lesage, F. Harel, P. Romeo, and J. Pressacco, "Imaging biomarkers in atherosclerosis trials," *Circ. Cardiovasc. Imaging*, vol. 4, no. 3, pp. 319–333, May 2011.

[4] T. L. Pinto and R. Waksman, "Clinical applications of optical coherence tomography," *J. Intervent. Cardiol.*, vol. 19, no. 6, pp. 566–573, Dec. 2006.

[5] M. Nahrendorf, F. A. Jaffer, K. A. Kelly, D. E. Sosnovik, E. Aikawa, P. Libby, and R. Weissleder, "Noninvasive vascular cell adhesion molecule-1 imaging identifies inflammatory activation of cells in atherosclerosis," *Circulation*, vol. 114, no. 14, pp. 1504–1511, Oct. 2006.

[6] L. Rouleau, R. Berti, V. W. K. Ng, C. Matteau-Pelletier, T. Lam, P. Saboural, A. K. Kakkar, F. Lesage, E. Rhéaume, and J.-C. Tardif, "VCAM-1-targeting gold nanoshell probe for photoacoustic imaging of atherosclerotic plaque in mice," *Contrast Media Mol. Imaging*, vol. 8, no. 1, pp. 27–39, Feb. 2013.

[7] J. Deguchi, M. Aikawa, C.-H. Tung, E. Aikawa, D.-E. Kim, V. Ntziachristos, R. Weissleder, and P. Libby, "Inflammation in atherosclerosis: visualizing matrix metalloproteinase action in macrophages in vivo," *Circulation*, vol. 114, no. 1, pp. 55–62, Jul. 2006.

[8] F. A. Jaffer, D.-E. Kim, L. Quinti, C.-H. Tung, E. Aikawa, A. N. Pande, R. H. Kohler, G.-P. Shi, P. Libby, and R. Weissleder, "Optical visualization of cathepsin K activity in atherosclerosis with a novel, protease-activatable fluorescence sensor," *Circulation*, vol. 115, no. 17, pp. 2292–2298, May 2007.

[9] C. Burtea, S. Laurent, O. Murariu, D. Rattat, G. Toubeau, A. Verbruggen, D. Vanssthertem, L. V. Elst, and R. N. Muller, "Molecular imaging of alpha v beta3 integrin expression in atherosclerotic plaques with a mimetic of RGD peptide grafted to Gd-DTPA," *Cardiovasc. Res.*, vol. 78, no. 1, pp. 148–157, Apr. 2008.

[10] C. Vinegoni, I. Botnaru, E. Aikawa, M. A. Calfon, Y. Iwamoto, E. J. Folco, V. Ntziachristos, R. Weissleder, P. Libby, and F. A. Jaffer, "Indocyanine green enables near-infrared fluorescence imaging of lipid-rich, inflamed atherosclerotic plaques," *Sci. Transl. Med.*, vol. 3, no. 84, p. 84ra45, 2011.

[11] S. Sethuraman, S. Mallidi, S. R. Aglyamov, J. H. Amirian, S. Litovsky, R. W. Smalling, and S. Y. Emelianov, "Intravascular photoacoustic imaging of atherosclerotic plaques: ex-vivo study using a rabbit model of atherosclerosis," *Proc. SPIE*, vol. 6437, no. 1, pp. 643729–643729-9, Feb. 2007.

[12] B. Wang, E. Yantsen, T. Larson, A. B. Karpiouk, S. Sethuraman, J. L. Su, K. Sokolov, and S. Y. Emelianov, "Plasmonic intravascular photoacoustic imaging for detection of macrophages in atherosclerotic plaques," *Nano Lett.*, vol. 9, no. 6, pp. 2212–2217, Jun. 2009.
[13] A. B. Karpiouk, B. Wang, and S. Y. Emelianov, "Development of a catheter for combined intravascular ultrasound and photoacoustic imaging," *Rev. Sci. Instrum.*, vol. 81, no. 1, p. 014901, Jan. 2010.
[14] B. Wang, J. L. Su, A. B. Karpiouk, K. V. Sokolov, R. W. Smalling, and S. Y. Emelianov, "Intravascular photoacoustic imaging," *IEEE J. Sel. Topics Quantum Electron.*, vol. 16, no. 3, pp. 588–599, Jun. 2010.
[15] B. Wang, A. Karpiouk, D. Yeager, J. Amirian, S. Litovsky, R. Smalling, and S. Emelianov, "Intravascular photoacoustic imaging of lipid in atherosclerotic plaques in the presence of luminal blood," *Opt. Lett.*, vol. 37, no. 7, pp. 1244–1246, Apr. 2012.
[16] D. Yeager, A. Karpiouk, B. Wang, J. Amirian, K. Sokolov, R. Smalling, and S. Emelianov, "Intravascular photoacoustic imaging of exogenously labeled atherosclerotic plaque through luminal blood," *J. Biomed. Opt.*, vol. 17, no. 10, pp. 106016–106016, 2012.
[17] K. Jansen, A. F. W. Van Der Steen, H. M. M. Ven Beusekom, J. W. Oosterhuis, and G. Ven Soest, "Intravascular photoacoustic imaging of human coronary atherosclerosis," *Opt. Lett.*, vol. 36, no. 5, pp. 597–599, Mar. 2011.
[18] K. Jansen, M. Wu, A. F. W. Ven Der Steen, and G. V. Soest, "Photoacoustic imaging of human coronary atherosclerosis in two spectral bands," *Photoacoustics*, vol. 2, no. 1, pp. 12–20, Mar. 2014.
[19] K. Jansen, A. F. Ven Der Steen, M. Wu, H. M. Van Beusekom, G. Springeling, X. Li, Q. Zhou, K. K. Shung, D. P. De Kleijn, and G. Van Soest, "Spectroscopic intravascular photoacoustic imaging of lipids in atherosclerosis," *J. Biomed. Opt.*, vol. 19, no. 2, pp. 026006–026006, 2014.
[20] B. Wang, A. Karpiouk, D. Yeager, J. Amirian, S. Litovsky, R. Smalling, and S. Emelianov, "In vivo intravascular ultrasound-guided photoacoustic imaging of lipid in plaques using an animal model of atherosclerosis," *Ultrasound Med. Biol.*, vol. 38, no. 12, pp. 2098–2103, Dec. 2012.
[21] F. A. Jaffer, M. A. Calfon, A. Rosenthal, G. Mallas, R. N. Razansky, A. Mauskapf, R. Weissleder, P. Libby, and V. Ntziachristos, "Two-dimensional intravascular near-infrared fluorescence molecular imaging of inflammation in atherosclerosis and stent-induced vascular injury," *J. Amer. Coll Cardiol*, vol. 57, no. 25, pp. 2516–2526, Jun. 2011.
[22] D. N. Stephens, J. Park, Y. Sun, T. Papaioannou, and L. Marcu, "Intraluminal fluorescence spectroscopy catheter with ultrasound guidance," *J. Biomed. Opt.*, vol. 14, no. 3, p. 030505, 2009.
[23] J. Bec, H. Xie, D. R. Yankelevich, F. Zhou, Y. Sun, N. Ghata, R. Aldredge, and L. Marcu, "Design, construction, and validation of a rotary multifunctional intravascular diagnostic catheter combining multispectral fluorescence lifetime imaging and intravascular ultrasound," *J. Biomed. Opt.*, vol. 17, no. 10, pp. 1060121–10601210, 2012.
[24] A. J. Dixon and J. A. Hossack, "Intravascular near-infrared fluorescence catheter with ultrasound guidance and blood attenuation correction," *J. Biomed. Opt.*, vol. 18, no. 5, p. 56009, May 2013.
[25] C. L. De Korte, G. Pasterkamp, A. F. W. Van Der Steen, H. A. Woutman, and N. Bom, "Characterization of plaque components with intravascular ultrasound elastography in human femoral and coronary arteries in vitro," *Circulation*, vol. 102, no. 6, pp. 617–623, Aug. 2000.
[26] Y. Majdouline, J. Ohayon, Z. Keshavarz-Motamed, M.-H. R. Cardinal, D. Garcia, L. Allard, S. Lerouge, F. Arsenault, G. Soulez, and G. Cloutier, "Endovascular shear strain elastography for the detection and characterization of the severity of atherosclerotic plaques: In vitro validation and in vivo evaluation," *Ultrasound Med. Biol.*, vol. 40, no. 5, pp. 890–903, May 2014.
[27] J. Fromageau, J.-L. Gennisson, C. Schmitt, R. L. Maurice, R. Mongrain, and G. Cloutier, "Estimation of polyvinyl alcohol cryogel mechanical properties with four ultrasound elastography methods and comparison with gold standard testings," *IEEE Trans. Ultrason., Ferroelectr., Freq. Control*, vol. 54, no. 3, pp. 498–509, 2007.
[28] R. L. Maurice, J. Fromageau, M.-H. Cardinal, M. Doyley, E. De Muinck, J. Robb, and G. Cloutier, "Characterization of atherosclerotic plaques and mural thrombi with intravascular ultrasound elastography: A potential method evaluated in an aortic rabbit model and a human coronary artery," *IEEE Trans. Inf. Technol. Biomed.*, vol. 12, no. 3, pp. 290–298, May 2008.
[29] R. Cubeddu, A. Pifferi, P. Taroni, A. Torricelli, and G. Valentini, "A solid tissue phantom for photon migration studies," *Phys. Med. Biol.*, vol. 42, no. 10, p. 1971, Oct. 1997.
[30] R. N. Razansky, A. Rosenthal, G. Mallas, D. Razansky, F. A. Jaffer, and V. Ntziachristos, "Near-infrared fluorescence catheter system for two-dimensional intravascular imaging in vivo," *Opt. Express*, vol. 18, no. 11, pp. 11372–11381, 2010.
[31] B. Li, M. Abran, C. Matteau-Pelletier, L. Rouleau, T. Lam, R. Sharma, E. Rhéaume, A. Kakkar, J.-C. Tardif, and F. Lesage, "Low-cost three-dimensional imaging system combining fluorescence and ultrasound," *J. Biomed. Opt.*, vol. 16, no. 12, p. 126010, 2011.
[32] F. Destrempes, M.-H. R. Cardinal, L. Allard, J.-C. Tardif, and G. Cloutier, "Segmentation method of intravascular ultrasound images of human coronary arteries," *Comput. Med. Imaging Graph.*, vol. 38, no. 2, pp. 91–103, Mar. 2014.

Maxime Abran received the B.Eng. degree in electrical engineering from École Polytechnique de Montréal, Montréal, QC, Canada, in 2011.

Currently, he is working toward the Ph.D. degree in the Department of Biomedical Engineering at École Polytechnique de Montréal, in association with the Montréal Heart Institute. His research interests include electronic design applied to biomedical applications, more specifically ultrasound and optical imaging.

Guy Cloutier (S'89–M'90–SM'07) received the B.Eng. degree in electrical engineering from the Université du Québec à Trois-Rivières, Trois-Rivières, QC, Canada, in 1984, and the M.Sc. and Ph.D. degrees in biomedical engineering from École Polytechnique de Montréal, Montréal, QC, Canada in 1986 and 1990, respectively.

From 1990–1992, he was a Postdoctoral Fellow at The Pennsylvania State University, State College, PA, USA, with Prof. K. Kirk Shung. He is Director of the Laboratory of Biorheology and Medical Ultrasonics at the University of Montréal Hospital Research Center (www.lbum-crchum.com), Professor and Director of Research at the Department of Radiology, Radio-Oncology and Nuclear Medicine of the University of Montréal, and Member of the Institute of Biomedical Engineering at the same Institution. His research interests are in quantitative ultrasound imaging of red blood cell aggregation; quasi-static and dynamic ultrasound elastography of atherosclerotic plaques, vascular aneurysms, deep vein thrombi, breast cancers, and liver steatosis; 3-D morphologic and hemodynamic assessment of lower limb arterial stenoses; and mathematical and biomechanical modeling. He has authored more than 150 peer-reviewed articles in these fields, holds 12 patents, and licensed two technologies.

Dr. Cloutier was recipient of the National Scientist Award of the Fonds de la Recherche en Santé du Québec (2004–2009). He is Associate Editor of IEEE TRANSACTIONS ON ULTRASONICS, FERROELECTRIC AND FREQUENCY CONTROL, Invited Associated Editor of *Medical Physics*, and member of the international advisory editorial boards of *Ultrasound in Medicine and Biology* and *Current Medical Imaging Reviews*.

Marie-Hélène Roy Cardinal received the B.Eng. degree in computer engineering from the École Polytechnique of Montréal, Montréal, QC, Canada, and the Ph.D. degree in biomedical engineering from the University of Montréal, Montréal, QC, Canada, in 2001 and 2008, respectively.

Since 2009, she has been working as a Research Associate in the Laboratory of Biorheology and Medical Ultrasonics of the University of Montréal Hospital Research Center. Her current research interests include intravascular ultrasound imaging, segmentation applied to ultrasound imaging, and atherosclerotic plaque characterization with ultrasound elastography.

Boris Chayer was born in Montréal, Canada, in 1975. He joined the engineering school of École de Technologie Supérieure, and he obtained a bachelor's degree in electrical engineering in 2001, and a master degree in Biomedical engineering in 2007.

He worked four years as a Research Assistant at Institut de Recherches Cliniques de Montréal, Montréal, QC, Canada, before he joined the University of Montréal Hospital Research Center in 2004. Currently, he is working in the Laboratory of Biorheology and Medical Ultrasonics on quantitative ultrasound imaging, elastography technics, and biomedical phantoms design.

Jean-Claude Tardif graduated from the University of Montréal, Montréal, QC, Canada, with a medical degree in 1987 and completed training in cardiology and research in Montréal and Boston, MA, USA, in 1994.

He is the Director of the Research Centre at the Montréal Heart Institute and Professor of Medicine at the University of Montréal. He has authored and/or coauthored more than 800 articles and abstracts in peer-reviewed publications including *The New England Journal of Medicine*, *The Journal of the American Medical Association*, *The Lancet*, *Circulation*, the *Journal of the American College of Cardiology*, the *European Heart Journal, Nature Genetics*, *Genes and Development*, the *British Journal of Pharmacology*, and *Cardiovascular Research*. In addition, he has written more than 30 book chapters (including Braunwald's textbook on heart disease) and has edited several books. He has given approximately 400 invited lectures around the world. He holds the Canada Research Chair in translational and personalized medicine and the University of Montréal endowed Research Chair in atherosclerosis. His research covers the molecular and genomic aspects of atherosclerosis and related diseases and also involves animal models, mechanistic and observational clinical studies as well as large international randomized clinical trials. He is or has been the international principal investigator or part of the study leadership of several large clinical trials in the field of atherosclerosis and other cardiovascular diseases.

Frédéric Lesage received the M.Sc. degree in applied mathematics and physics from the Univerisity of Cambridge, Cambridge, U.K., and the Ph.D. degree in physics from the University of Paris-Sud, Orsay, France.

Currently, he is a Researcher at the Montréal Heart Institute (MHI), Montréal, QC, Canada, and has been a Professor of electrical engineering at the École Polytechnique de Montréal since 2005, specializing in the development of optical imaging techniques. Before arriving at Polytechnique, he studied and held industry positions in bioimaging. Presently, he manages a laboratory of 20 people. His research activities deal with the development of novel imaging techniques for neural imaging. These techniques are used with humans (diffuse optical imaging of the brain during cognitive tasks and study of the neuronal metabolism) and small animals (study of neuro-degenerative diseases by means of transgenics and molecular fluorescent probes). He is particularly interested in the question of brain and vascular aging. He has performed a number of studies on brain aging using various optical imaging techniques such as diffuse optical tomography, near-infrared spectroscopy, optical coherence tomography, and two-photon microscopy.